J Solid State Electrochem (2012) 16:1429–1445
DOI 10.1007/s10008-011-1540-3

ORIGINAL PAPER

Photocatalytic degradation on Disperse Blue with modified nano-TiO_2 film electrode

Wenwei Tang · Qian Wang · Xinping Zeng · Xiaoying Chen

Received: 17 February 2011 / Revised: 13 July 2011 / Accepted: 20 August 2011 / Published online: 9 September 2011

Abstract Sol–gel and dip-coating methods were used to prepare the modified nano-TiO_2 film electrode; its photocatalytic and electrochemical properties were investigated under both UV light and sunlight for the degradation of Disperse Blue. The results showed that the effect of co-doping metal and non-metal ions was better than that of single metal ion doping or no doping. Y–F co-doping could better take advantage of sunlight so as to decrease the energy gap of semiconductor and to improve the utilization of visible light, while Ce–F co-doping served to separate photo-generated h^+/e^- pairs, which resulted in better degradation of dye under UV light. The grain size of prepared electrode was from 15 to 25 nm, and nano particles were arranged smoothly as well as closely with each other, confirming to be an effective binder. The final decolorization extents reached 44.43% under sunlight and 96.86% under UV light within 30 min, respectively.

Keywords Modified nano-TiO_2 film electrode · Sol–gel · Photocatalysis · Disperse Blue

Introduction

Titanium dioxide (TiO_2) serves as one of the most promising photocatalytic materials in the area of environmental protection, especially in the heterogeneous photocatalytic field [1]. That is to say, a better understanding and improvement of the reaction could enable it to be widely applied in industry, such as the treatment of effluent of dyes. The surface of TiO_2 is excited by UV light so as to generate conduction band electron (e^-) and valence band hole (h^+). h^+ has a strong ability to obtain electron and to generate strong oxidability—it can oxidize OH^- and H_2O absorbed on surface to ·OH; meanwhile, e^- can also react with absorbed O_2 to form active oxygen like $\cdot O_2^-$ which in combination with ·OH together participate in redox reactions [2]. The superiorities of TiO_2, such as operation simplicity, moderate reaction conditions, high degradation efficiency, easy automation, no secondary pollution, etc., are the hotspots and highlights that win researchers' attention and favors in recent years [3].

However, two main drawbacks largely limit the industrial application of this photocatalytic technology: (1) the energy gap is too large (3.2 eV) so it can only be exited effectively under ultraviolet irradiation where the wavelength is smaller than 380 nm, but there is only 4% of UV light in sunlight; therefore, TiO_2 responds weakly to sunlight and (2) the lifespan of h^+/e^- pairs is not long enough to lower the quantum efficiency [4, 5].

The way to promote the efficiency of photocatalysis includes the improvement through preparation and the modification by some other elements such as transition metal, noble metal, base metal, or even non-metal. Modification can not only improve the photocatalytic activity of TiO_2 towards the degradation on organic pollutants but also result in the expansion of photosensitivity to the visible light region [6]. Marta Mrowetz et al. [7] found that nitrogen doping could extend the absorption of TiO_2 into the visible light region. Michael R et al. [8] conducted a systematic study of metal ion doping in quantum-sized TiO_2 and found that the concentration of dopant greatly influenced the energy level because of a complex function. Riassetto D et al. [9]

W. Tang · Q. Wang · X. Chen
Department of Chemistry, Tongji University,
Room 437, #1239 Siping Rd,
Shanghai 200092, China

W. Tang
e-mail: tangww@tongji.edu.cn

X. Zeng (✉)
School of Life Sciences and Technology, Tongji University,
#1239 Siping Rd,
Shanghai 200092, China
e-mail: zengxp@tongji.edu.cn

successfully prepared Pt-doped nano-TiO_2 particles to improve the photocatalytic properties. F´elix G et al. [10] also discovered that Ce doping could significantly enlarge the surface area and lower the energy gap.

In this paper, sol–gel method was used to prepare modified nano-TiO_2 film electrode by both single metal ion doping and co-doping metal and nonmetal ions. The properties of electrode were optimized via adjustment of several parameters, and Disperse Blue (DB) solution served as the refractory wastewater for degradation experiment decolorized by prepared electrode under both sunlight and UV light.

Materials and methods

Reagents

Disperse Blue from Shanghai Dyeing Plant, ethanolamine ($HOCH_2CH_2NH_2$), tetrabutyl titanate (TBTA), acetylacetone ($C_5H_8O_2$), isopropanol ($(CH_3)_2CHOH$), polyethylene glycol (PEG4000), yttrium nitrate hexahydrate ($Y(NO_3)_3{\cdot}6H_2O$), cerium nitrate hexahydrate ($Ce(NO_3)_3{\cdot}6H_2O$), sodium fluoride (NaF), etc. were all of analytical purity. TA1-type Ti sheet was chosen as Ti substrate (with thickness of 0.5 mm) from Shanxi Ti Company.

Apparatus

The range of apparatus used included a self-made photocatalytic reactor (500 W UV lamp)—the device is shown in Fig. 1; in via confocal microscopic Raman spectroscopy (Renishaw in Britain); S-4800 scanning electron microscope (Hitachi in Japan); AUTOLAB model PGSTAT30 (Metrohm in Switzerland); D8 ADVANCE X X-ray diffractometer (Bruker in Germany); 8453 UV–vis spectrometer (Agilent in the USA); and self-made elevator with slow velocity.

Preparation of nano-TiO_2 film electrode

Firstly, 5 mL isopropanol was added into 10 mL TBTA, while a small amount of acetylacetone was used as inhibitor to slow down the hydrolysis of TBTA. After vigorous stirring for 0.5 h, component A was prepared. A thimbleful of distilled water was added into 2.5 mL isopropanol where ethanolamine served as regulator to get component B; 5% (wt%) PEG was a thickener here to avoid the agglomeration of particles and increase hydrophilicity and was mixed with 2.5 mL isopropanol to obtain component C. Proportional amounts of $Y(NO_3)_3{\cdot}6H_2O$, $Ce(NO_3)_3{\cdot}6H_2O$, and NaF were added and dissolved into component C, respectively, at the same time. Then, B was added dropwise into C under vigorous stirring, and A was also added dropwise into BC intermixture, after stirring for 0.5 h and aging overnight, and then stably translucently and homogeneously yellow TiO_2 sol was prepared for further usage.

Polished ultrasonic was cleaned in detergent and acetone, respectively, and then detarnished under acid etching followed by washing with distilled water. Ti substrate (2×3 cm) was sealed under anhydrous ethanol [11]. Dip-coating method was applied in this paper for the preparation of modified electrode to optimize the properties because of its low cost and controllability. Ti sheet was dipped vertically into the sol solution and elevated under slow speed then dried under an infrared lamp for 10 min and annealed at 500 °C for 10 min in a muffle furnace after five times of dip-coating to make sure that the coating layer was completely oxidized. The process was repeated three times while the last annealing time increased to 90 min to acquire modified anatase TiO_2 electrode.

Experiment for photocatalysis

The reaction was operated in a self-made reactor. A 500-W UV lamp with a main emission at 254 nm as the external

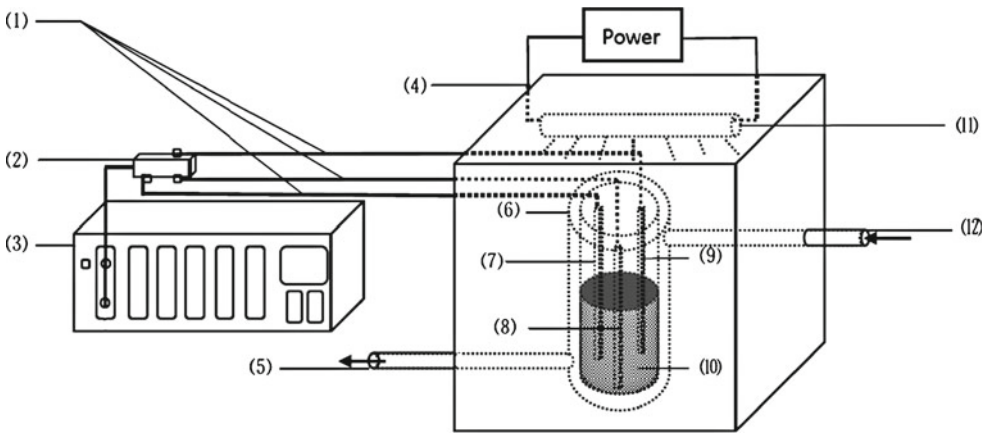

Fig. 1 Self-made photocatalytic reactor

(1) Wire, (2) Connector, (3) Autolab, (4) Reactor, (5) Condensate outlet, (6) Beaker, (7) SCE, (8) TiO_2 electrode, (9) Pt electrode, (10) DB solution, (11) UV lamp, (12) Condensate inlet

light source was suspended on the side wall of the reactor, and the whole degradation process was conducted in a beaker containing 50 mL 100 mg/L DB solution and connected to a condensate pipe with continuing cooling water. Modified nano-TiO_2 film electrode served as the working electrode and Pt electrode acted as counter electrode, whereas a saturated calomel electrode was used as reference electrode. The degradation was operated under sunlight and UV light for 30 min, respectively. UV–vis spectrometer was used for whole-wavelength scanning and the maximum absorptive wavelength was 567 nm. The absorbance values before and after the reaction were recorded as A_0 and A. The calculation for decolorization extent on DB could be:

$$\eta = (A_0 - A)/A_0 \times 100\% \quad (1)$$

Results and discussion

Optimization of parameters for the preparation of modified electrode

Influence of doping amount of $Ce(NO_3)_3{\cdot}6H_2O$ on electrode

The doping of elements from lanthanide could localize the photo-generated electrons and holes on lanthanide and TiO_2, respectively, so as to inhibit the recombination of the pairs. In this paper, $Ce(NO_3)_3{\cdot}6H_2O$ was the dopant for Ce^{3+} doping. The molar ratios between Ti and Ce were 100:0, 100:0.5, 100:1.0, and 100:1.5, respectively.

Figure 2 exhibited the XRD patterns of modified TiO_2 electrodes under different intermingled quantities of Ce^{3+}. It was showed that Ce doping by no means changed the anatase phase of TiO_2, and no other oxidants containing Ce element were detected. However, the peak intensity of anatase phase (101) of TiO_2 (2θ=25°) decreased with the doping quantities of Ce^{3+}. It was contributed to the fact that [12–14] Ce^{3+} was uniformly distributed in the system to form stable TiO_2 sol. The radius of Ce^{4+} was 0.092 nm, which was larger than that of Ti^{4+} (0.068 nm). Therefore, Ce^{4+} cannot find an easy access to the lattice of TiO_2 but only be bonded with the surface of TiO_2 grains through Ti–O–Ce bonds then inhibited the further growth of grain size. In addition, the Ce-4f orbit was in the most stable state while completely empty, half full, or fully full, which meant that Ce^{4+} found itself easy to obtain e^- and become Ce^{3+}. Hence, the following reaction might have happened under annealing so as to generate large amount of valences [15, 16]:

$$2Ce^{4+} + O^{2-} \rightarrow 2Ce^{3+} + 1/2O_2 + \text{valence} \quad (2)$$

At the same time, it could also be seen from the figure that the more the doping of Ce element, the broader the peak shape of XRD patterns, which implied the smaller grain size of nano particles. The calculation from Scherrer equation ($D_{hkl} = \kappa \times \lambda/(\beta_{hkl} \times \cos\theta)$) in Table 1 was in accordance with the conclusion above.

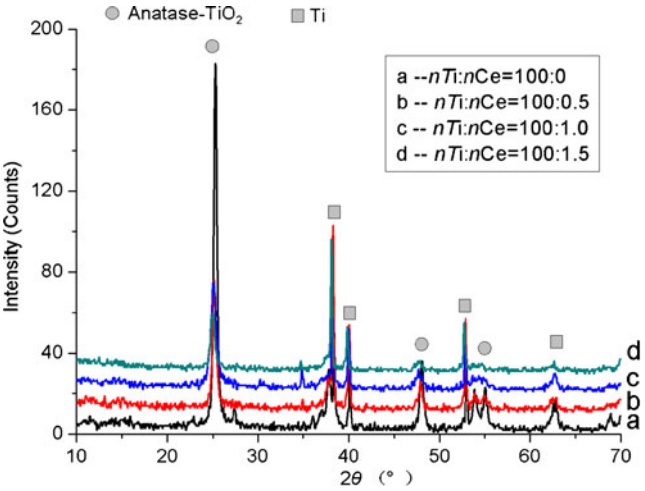

Fig. 2 XRD patterns under different molar ratios between Ti and Ce

The prepared sol solution under different molar ratios between Ti and Ce was dried for 2 h in an oven firstly and then annealed at 500 °C for 90 min in a muffle furnace. The TiO_2 powder obtained was experimented for ultraviolet–visible diffuse reflection, and energy gap was also calculated by the following formula:

$$E_g = 1,240/\lambda \quad (3)$$

where E_g was the energy gap (eV) of TiO_2 and λ was the wavelength of absorption edge (nm). The figure was shown in Fig. 3 and the results were exhibited in Table 2. The data and curves implied that single Ce-doping cannot improve the photosensitivity efficiency of sunlight well and make the red-shift because of the slightly bigger energy gap.

The modified powders were also under Fourier-transformed infrared (FT-IR) test and the results were shown in Fig. 4. In the FT-IR spectrum, 500~1,000 cm^{-1} were the nonsymmetrical vibration of the stretching vibration of Ti–O bond; 700 cm^{-1} was the symmetric stretching vibration of Ti–O–Ti bond; 1,600 cm^{-1} was the bend vibration of hydroxy while 3,100–3,700 cm^{-1} were the symmetric stretching vibration of hydroxyl (in this paper, it was resulted from butyl alcohol derived from the hydrolysis of TBTA) [17, 18]. The adding of PEG enabled the bonding between CH_2-O side chain and Ti- to form the

Table 1 Grain size of electrode under different molar ratios between Ti and Ce

*n*Ti/*n*Ce	100:0	100:0.5	100:1.0	100:1.5
Grain size, nm	19	19	17	14

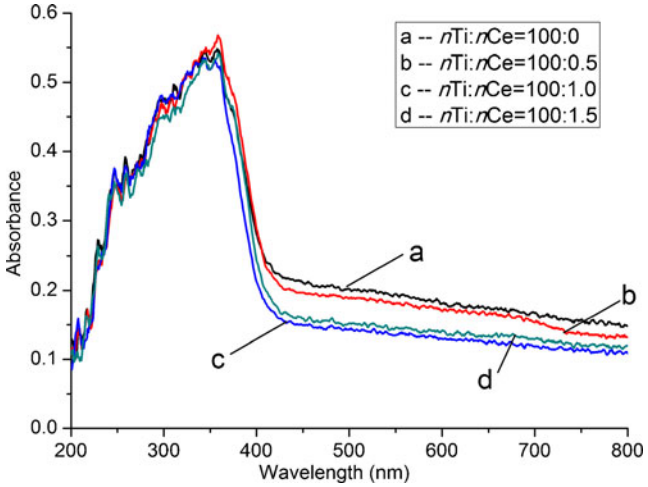

Fig. 3 UV–vis diffuse reflection spectrum under different ratios between Ti and Ce

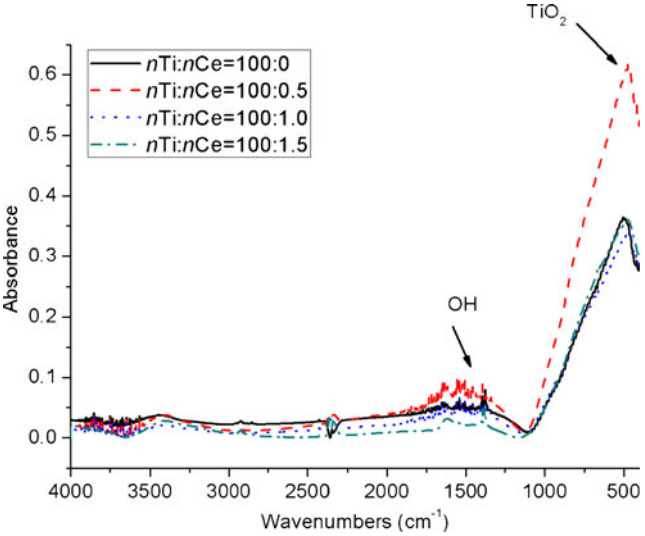

Fig. 4 FT-IR spectrum of Ce-doping TiO_2 powders

structure like CH_2–O–Ti because of its compatibility, dispersibility, stability as well as viscosity, and it could be completely decomposed under 250 °C [13]. No matter how much Ce was doped, no other place appeared as the absorption peak but at 500 to 1,000 cm^{-1}. This proved that the PEG served as the thickener and during the preparation other organics were all decomposed, volatized, or completely burnt except TiO_2.

The open-circuit potential (OCP) was a mixed potential of all the redox potentials in the solution, at the surface, and at the interface, and its trend absolutely implied the change of the surface of the electrode [20]. In this research, Autolab was used to observe the variation of electrodes prepared under different molar ratios between Ti and Ce, and the relationship between OCP and time under UV light was also discussed. The OCP dropped down to much more negative values when the electrode was irradiated with UV light as a result of the sudden generation of photo-generated h^+/e^- pairs [19]. The detailed process can be described as follows: the UV lamp was turned off for the first 50 s then turned on for the next 50 s and turned off for the last 50 s. The values of potential both before the light's turning on and after its turning off were recorded and subtracted; the results were listed in Fig. 5. After irradiation for a short time, the balance rate between creation and depletion of photo-generated carriers was obtained. The value of OCP tended to be stable and a steady state of photoreactions was attained on nano-TiO_2 film electrodes [20]. Under the doping molar ratio *n*Ti/*n*Ce=100:0.5, the electrode reached the largest OCP at 0.6508 V. Its response to UV lamp was more notable than the others; however, excessive doping of Ce would lead to the excessive distortion of lattice and changes of cell constant so as to lower the response to UV light. The OCP value in this paper was twice as large as what Li M C [20] had done while four times as large as what Shuhu Xiao [21] had researched.

In addition, the electrochemical impedance spectroscopy (EIS) response of TiO_2 electrode under both sunlight and UV light at OCP was also operated in this research. Under UV light, the amount of photo-generated electrons would be much more than that of under sunlight. Therefore, the resistance would be reduced so that the arc radius on the EIS Nyquist plot shrank [19]. In this paper, the high and low frequencies were 1,000,000 and 1 Hz, respectively, for EIS test because of the better Nyquist arc that the electrode exhibited under this condition. The results can be seen in Fig. 6. The doping of Ce element cannot lower the

Table 2 Energy gap under different ratio between Ti and Ce

*n*Ti/*n*Ce	100:0	100:0.5	100:1.0	100:1.5
Energy gap, eV	2.78	2.83	2.90	2.88

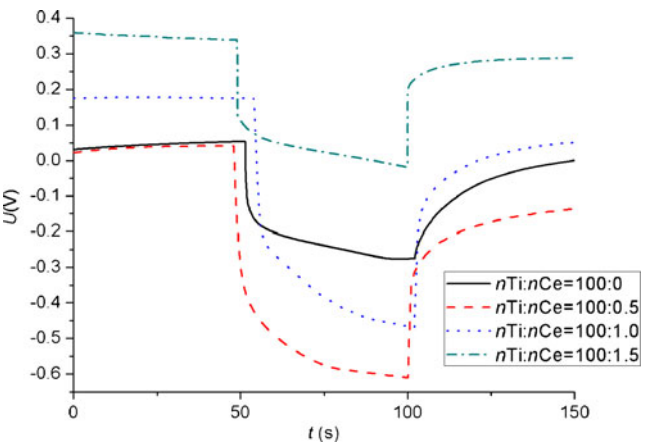

Fig. 5 OCP-Ce-doping molar ratio relationship under UV radiation

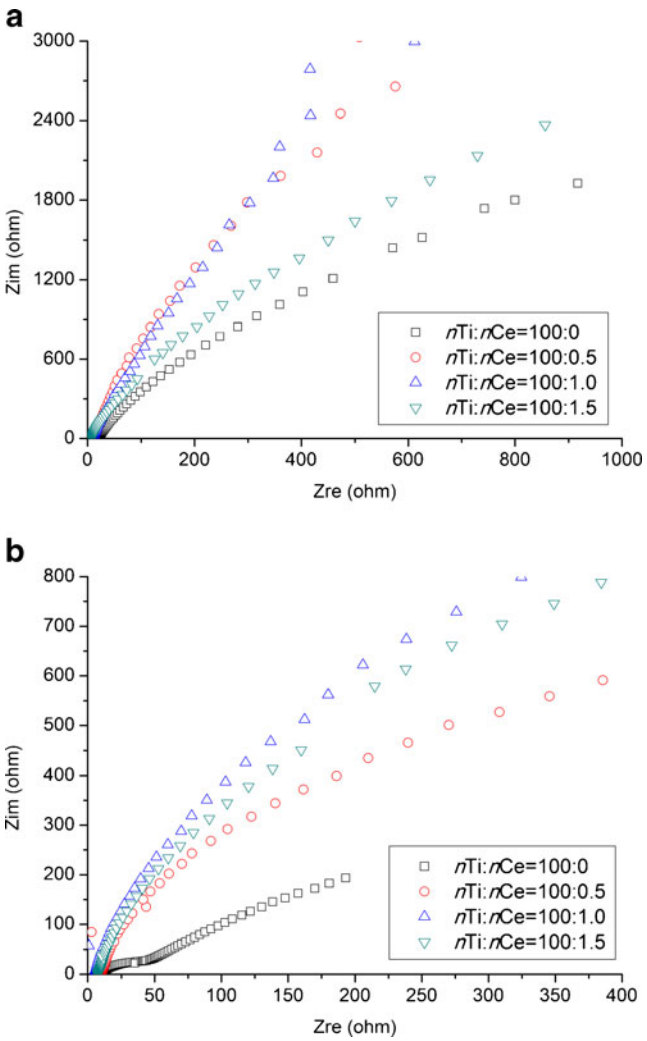

Fig. 6 EIS of electrode under different Ce-doping molar ratio

resistance of electrode whether it was under sunlight or UV light, which was in accordance with the conclusion from UV–vis diffuse reflection. However, the resistance under UV light when the molar ratio was *n*Ti/*n*Ce=100:0.5 was smaller than the other doping quantities.

Given all that, the molar ratio *n*Ti/*n*Ce=100:0.5 was chosen as the proper molar ratio for Ce-doping.

Influence of doping amount of $Y(NO_3)_3{\cdot}6H_2O$ on electrode

The doping of elements from transition element could refine the grain size of nano TiO_2 and serve as the potential trap for inhibition between photo-generated hole and electron; it resulted from the charge transfer between electrons on d orbital of doping element and electrons on conduction or valence band of TiO_2. In this paper, Y $(NO_3)_3{\cdot}6H_2O$ was the dopant for Y-doping. The molar ratios between Ti and Y were 100:0, 100:0.5, 100:1.0, and 100:1.5, respectively.

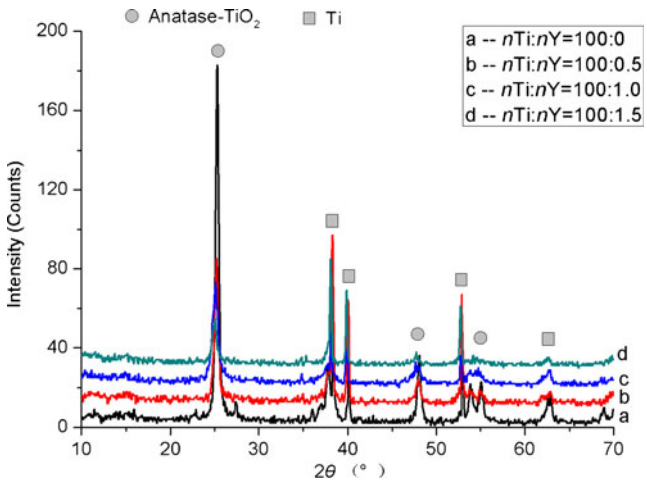

Fig. 7 XRD patterns under different molar ratio between Ti and Y

The structure change was due to the radius of doping element and its electrical charge. Dopant could replace Ti^{4+} or occupy the space among lattice node [22]. Figure 7 showed the XRD patterns of modified TiO_2 electrodes under different intermingled quantities of Y^{3+}. It was shown that Y-doping in no way changed the anatase phase of TiO_2, and no other oxidants containing Y element were detected. However, the peak intensity of anatase phase (101) of TiO_2 (2θ=25°) decreased with the doping quantities of Y^{3+}. It might be contributed to the fact that [23] the little amount of Y enabled a uniform distribution in the sol system without detection by XRD or resulted from the reason that [24, 25] the radius of Y^{3+} was 0.088 nm, which was larger than that of Ti^{4+} (0.068 nm). Therefore, Y^{3+} rendered the nano lattice to form Ti–Y_xO_y–TiO_2 solid solution, which meant that Y^{3+} found itself an access to the lattice of TiO_2 so as to lead its distortion and weaken the peak intensity of anatase phase. Also, the more the doping quantity of Y, the broader the peak shape of XRD patterns. The phenomena was convinced from the calculation of grain size from the Scherrer equation shown in Table 3, which implied that the more the doping of Y^{3+}, the smaller the grain size of nano particles.

The prepared sol solution under different molar ratios between Ti and Y were dried for 2 h in an oven firstly and then annealed at 500 °C for 90 min in a muffle furnace. The obtained TiO_2 powder was experimented for ultraviolet–visible diffuse reflection (Fig. 8), and the data of energy gap were also shown in Table 4.

Table 3 Grain size of electrode under different molar ratio between Ti and Y

*n*Ti/*n*Y	100:0	100:0.5	100:1.0	100:1.5
Grain size, nm	19	19	15	11

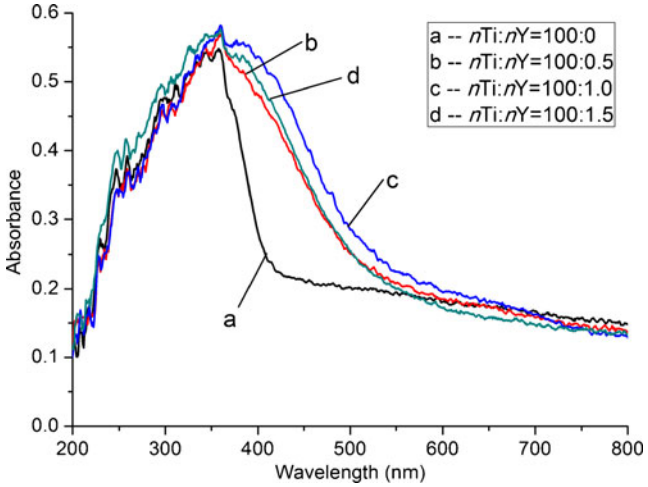

Fig. 8 UV–vis diffuse reflection spectrum under different molar ratio between Ti and Y

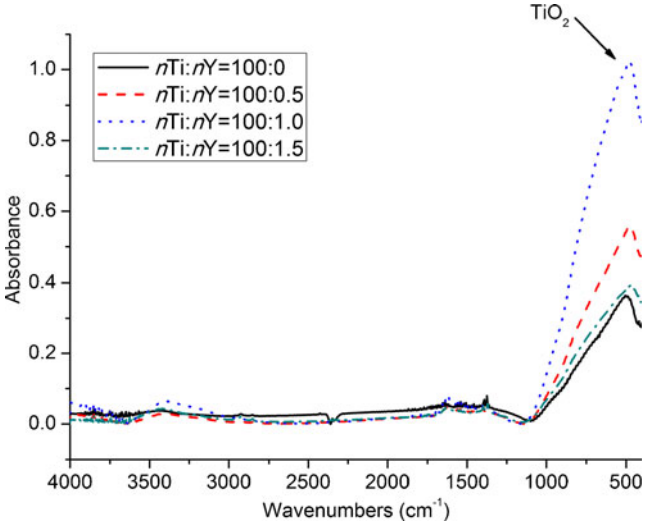

Fig. 9 FT-IR spectrum of Y-doping TiO_2 powders

The figure showed that Y, as a transition element, could effectively expand the photosensitivity of TiO_2 into the visible light region, and the response range increased to 500 nm compared to the former 345 nm. It was because Y had a larger range of light adsorption range, and Y-doping rendered the original TiO_2 to become photosensitive and form a new energy level to effectively adsorb sunlight [26]. Lattice distortion from doping would form strain energy in order to compensate this energy. Oxygen atoms from the TiO_2 surface found for themselves an easy way to escape from the lattice so as to take effect as h^+ trap, lower the recombination of h^+/e^- pairs, and improve photo-catalytic activity [26]. Although Y-doping can improve sunlight efficiency, there still existed an optimal doping quantity because excessive doping also led to the excessive distortion of lattice and the decrease of photosensitivity. Data in Table 4 also explained that the energy gap of TiO_2 could get the lowest value at nTi/nY=100:1.0.

The FT-IR test and the results were shown in Fig. 9. No matter how much Y was doped, no other place was the absorption peak but at 500 to 1,000 cm^{-1}. The figure proved that the PEG served as the thickener and during the preparation other organics were all decomposed, volatized, or completely burnt except TiO_2.

OCP test was also experimented here. The values of potential both before the light's turning on and after its turning off were recorded and subtracted, and the results were listed in Fig. 10. The figure exhibited that under the doping molar ratio nTi/nY=100:1.0, the electrode got the biggest OCP at 0.6051 V. Its response to UV lamp was also more notable than others, and excessive doping of Y would lead to the excessive accumulation on Ti–Y_xO_y–TiO_2 solid solution. The accumulated electrons generated electric field to capture holes, which meant that excessive Y-doping became a recombination center of h^+/e^- pairs and resulted in a decrease of photo-catalytic activity.

In addition, EIS response of modified TiO_2 electrode under both sunlight and UV light at OCP was also operated in this research. The results can be seen in Fig. 11. The Nyquist arc still proved the homogeneity doping [27]. The doping of Y element enabled the decrease of the Nyquist arc so as to decrease the resistance of electrode under sunlight, and the optimal doping quantity was nTi/nY=100:1.0 because of refinement of grain size and decrease of resistance among particles; on the other side, the resistance

Table 4 Energy gap under different molar ratio between Ti and Y

nTi/nY	100:0	100:0.5	100:1.0	100:1.5
Energy gap, eV	2.78	2.11	2.09	2.13

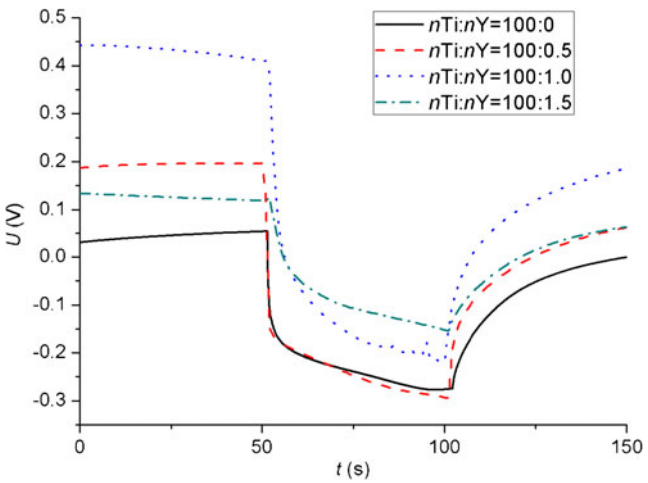

Fig. 10 OCP-Y-doping molar ratio relationship under UV radiation

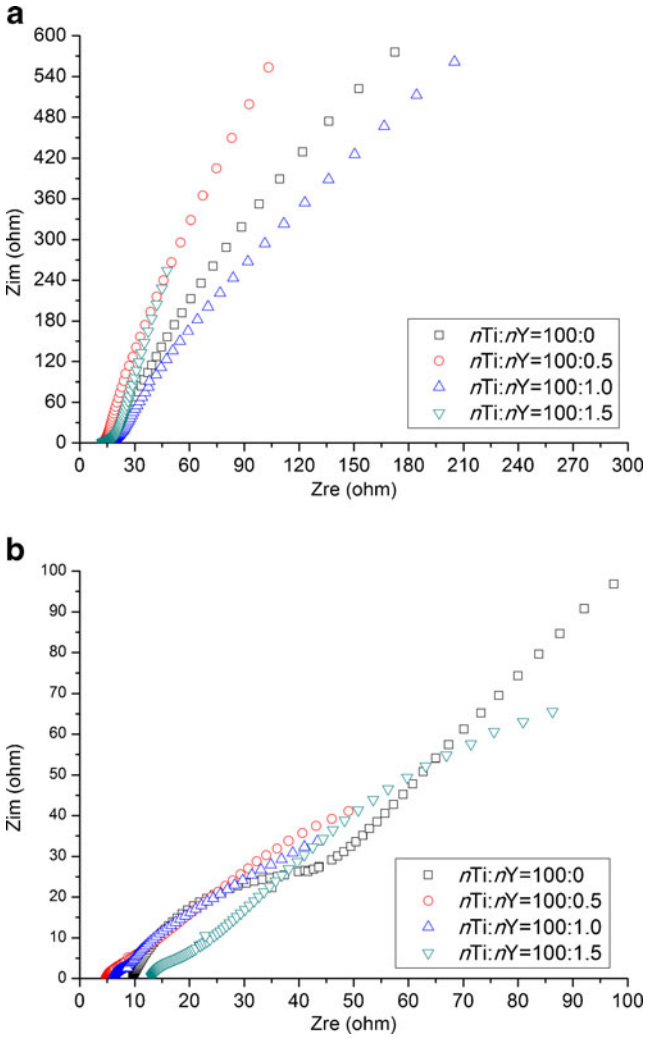

Fig. 11 EIS of electrode under different Y-doping molar ratio

of electrode under UV light was a little bit larger than that of no doping, which meant that Y-doping cannot effectively expand the use of UV light.

Therefore, nTi/nY=100:1.0 was chosen as the proper molar ratio for Y-doping.

Influence of co-doping on modified electrode

Researchers have proved that [28] single metal ion doping could improve the photocatalytic efficiency but not expand the photosensitivity to the visible light region, whereas non-metal doping can enable the photocatalytic material TiO_2 to respond to the visible light so as to effectively take advantage of sunlight. In addition, co-doping of metal and non-metal elements can produce a synergetic effect [29–31]. On one hand, non-metal element served as the inhibitor of photo-generated h^+/e^- pairs; on the other hand, metal element played a role in expanding the photosensitivity range. Documents had also illustrated that [12, 32] F^- doping can form Lewis acid and enhance surface acidity. The acids formed can react with π^- charged aromatic compounds to form new active sites and improve the photocatalytic efficiency of TiO_2. At the same time, photocatalysis was the synergism between direct and indirect oxidation. Surface fluorination could not only decrease the recombination of h^+/e^- but also increase the mass transfer among organics in the solution so as to degrade them into intermediates and then the final products [33]. As a result, co-doping of Ce–F and Y–F was investigated in this paper for modification of TiO_2 electrode.

Influence of co-doping an amount of $Ce(NO_3)_3{\cdot}6H_2O$ and NaF on electrode

The doping molar ratios between Ti and F were nTi/nF= 1:0.1, 1:0.5, 1:1.0, and 1:1.5, respectively. After one-night aging, only the sample at nTi/nF=1:0.1 was stable while others formed white precipitates. The stable sample was used for dip-coating at 500 °C and annealing for 90 min and then the modified electrode was prepared.

The XRD patterns of the electrode were shown in Fig. 12. Ce–F co-doping had not changed the anatase phase of TiO_2 but weakened the peak intensity, which meant that Ce and F were uniformly distributed in a sol system. At the same time, the calculation for grain size was listed in Table 5, which meant that co-doping cannot show the effect of refining the grain size.

The FT-IR test was also experimented here. The results were shown in Fig. 13. The absorption peak from 500 to 1,000 cm^{-1} was assigned to TiO_2. The wavelength range from 3,200 to 3,600 cm^{-1} proved the weak existence of hydroxy derived from the hydrolysis of TBTA. The presence of surface hydroxy did good to the improvement of photocatalytic oxidation. No other absorption peak can be found here.

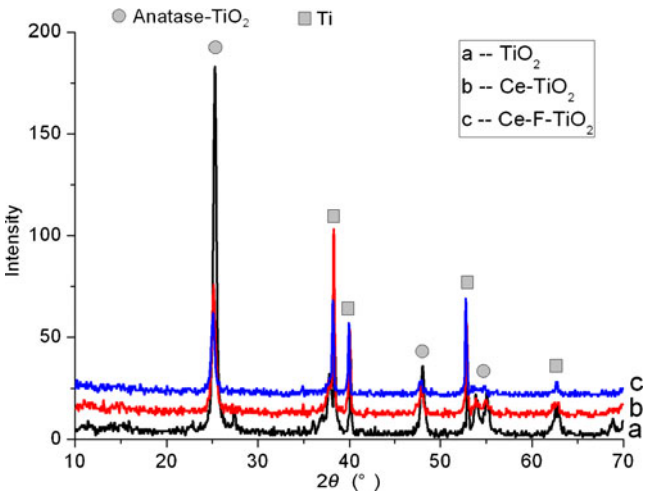

Fig. 12 XRD patterns of TiO_2, Ce-doping TiO_2 and Ce–F co-doping TiO_2 electrodes

Table 5 Grain size of TiO_2, Ce-doping TiO_2, and Ce–F co-doping TiO_2 electrodes

Electrode	TiO_2	Ce-doping TiO_2	Ce–F co-doping TiO_2
Grain size, nm	19	19	20

The modified powders were also tested under ultraviolet–visible diffuse reflection and the result was shown in Fig. 14 while the energy gap values are listed in Table 6. The absorption spectrum slightly expanded to the visible light region and the energy gap was lower than that of single doping or without doping. Ce–F co-doping was effective in generating more photo-generated h^+/e^- pairs [34].

EIS test was performed both under sunlight and UV light, and the results were shown in Fig. 15. Ce–F co-doping did not show marked improvement under sunlight; the resistance of co-doping electrode was still large. However, under UV light, the resistance of co-doping electrode was definitely smaller than under other conditions, which was consistent with the conclusion from ultraviolet–visible diffuse reflection.

OCP was also tested here under UV light and the result was shown in Fig. 16. The figure showed that the OCP obtained the biggest value at 0.7193 V under co-doping. Its response to UV lamp was also more notable than single doping and no doping, proving that F can take effect on the separation of photo-generated h^+/e^- pairs so as to improve the photosensitivity of the electrode.

Linear sweep voltammetry (LSV) was used for investigating the electrochemical properties as well. The conclusion can be seen as in Fig. 17. Ce–F co-doping did not show its advantages under sunlight on account of no significant difference among currents with the increase of voltage but reflected a notable performance under UV light

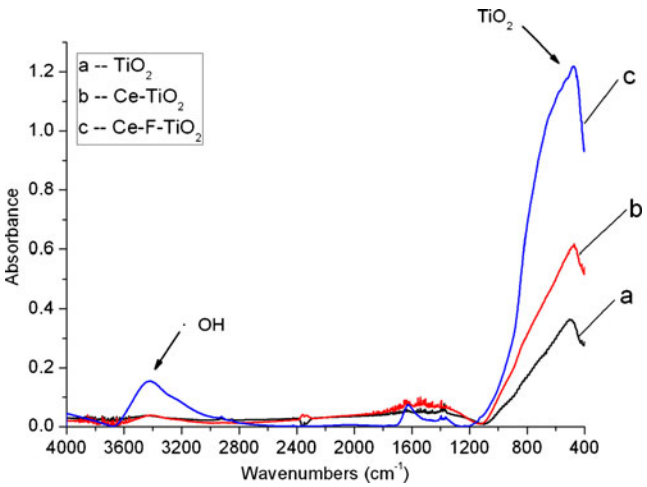

Fig. 13 FT-IR spectra of electrode under doping and co-doping of Ce and Ce–F

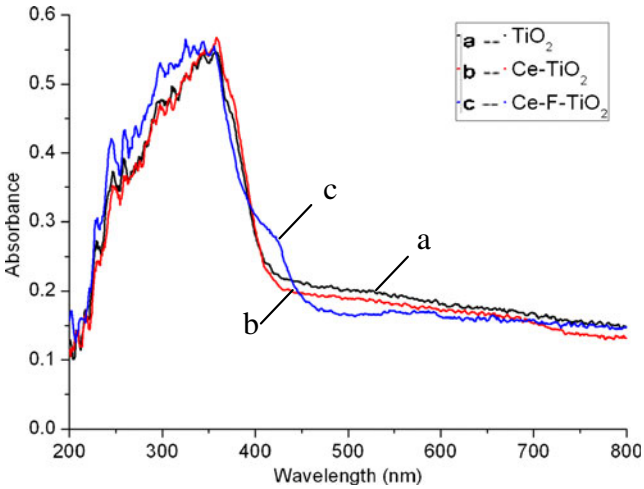

Fig. 14 UV–vis spectrum under different co-doping of Ce and Ce–F

irradiation, which meant that Ce–F co-doping can effectively improve photo-quantum efficiency.

Scanning electron microscope (SEM) was used for morphology in this paper, and the pictures were displayed in Fig. 18. The results illustrated that under a magnification of × 2,000, the surface of a single Ce-doping electrode was much smoother and less cracked than that of under Ce–F co-doping or without doping, where the co-doping and no-doping electrode appeared with a typical cracking "island" structure; under the magnification of × 100,000, the grain size of Ce single doping electrode exhibited more refined particles with a value from 15 to 20 nm, where the Ce–F co-doping rendered the lattice distortion more severe so as to make the grain size a little bit larger. However, the arrangement of particles was still dense and uniform and resulted in an increase of active sites and specific surface areas; on the contrary, the grain size of the electrode without doping was not that uniform and more cracks can also be seen. Besides, no other kinds of oxide were found on the surface of electrodes to manifest that Ce^{3+} entered into the TiO_2 lattice.

Given all that, the proper molar ratio of a modified electrode with co-doping of Ce and F should be *n*Ti/*n*Ce= 100:0.5 and *n*Ti/*n*F=1:0.1.

Influence of co-doping amount of $Y(NO_3)_3{\cdot}6H_2O$ and NaF on electrode

The doping molar ratios between Ti and F were *n*Ti/*n*F= 1:0.1, 1:0.5, 1:1.0, and 1:1.5, respectively. The other

Table 6 Energy gap under co-doping of Ce and Ce–F

Electrode	TiO_2	$Ce–TiO_2$	$Ce–F–TiO_2$
Energy gap, eV	2.78	2.83	2.55

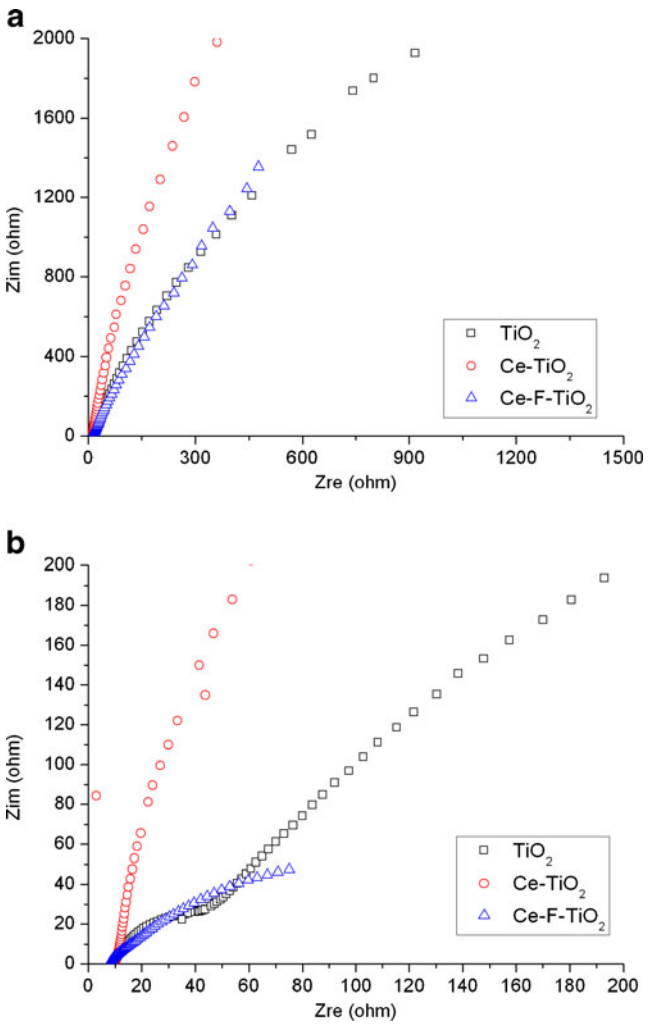

Fig. 15 EIS of electrode under co-doping of Ce and Ce–F

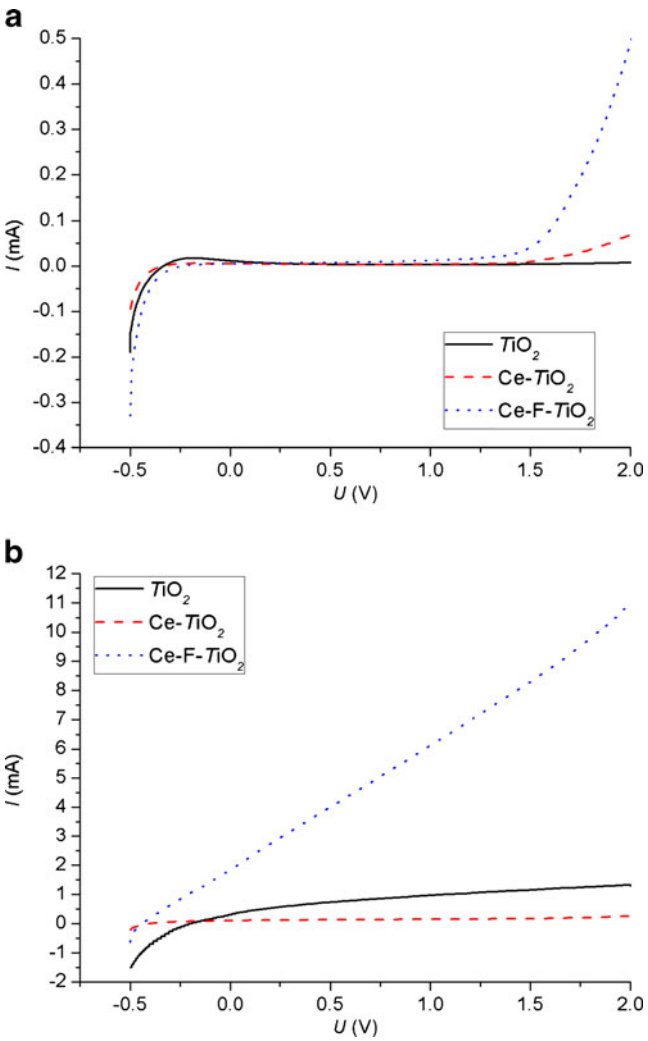

Fig. 17 LSV of electrode under co-doping of Ce and Ce–F

operations for preparing the sol system were totally the same as described before. After one-night aging, only the sample at nTi/nF=1:0.1 was stable while others formed white precipitates. The stable sample was used for dip-coating with 500 °C and annealing for 90 min and modified electrode was prepared.

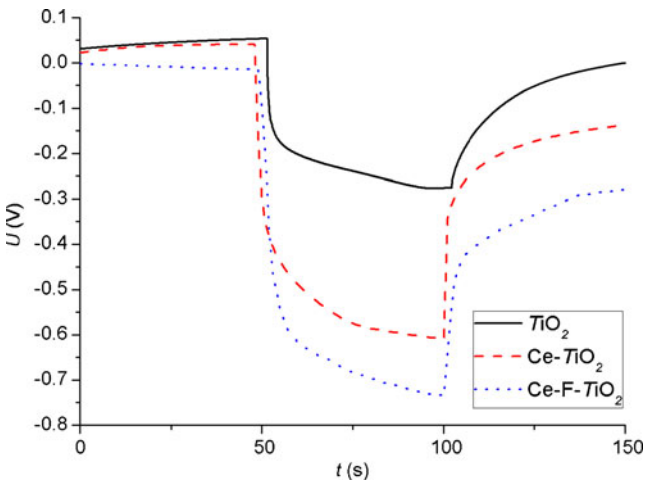

Fig. 16 Relationship between OCP and Ce-doping or Ce–F co-doping

The XRD patterns of electrode were shown in Fig. 19. Y–F co-doping had not changed the anatase phase of TiO_2 but weakened the peak intensity, which proved the uniform distribution of Y and F in the sol system. At the same time, the calculation for grain size was listed in Table 7, which meant that doping cannot take advantage of refining the grain size.

The FT-IR test was also experimented here; the results were shown in Fig. 20. the absorption peak from 500 to 1,000 cm^{-1} was assigned to TiO_2. The wavenumber range from 3,200 to 3,600 cm^{-1}, which proved the weak existence of hydroxy derived from the hydrolysis of TBTA. The presence of surface hydroxy did good to the improvement of photocatalytic oxidation. No other absorption peak can be found here.

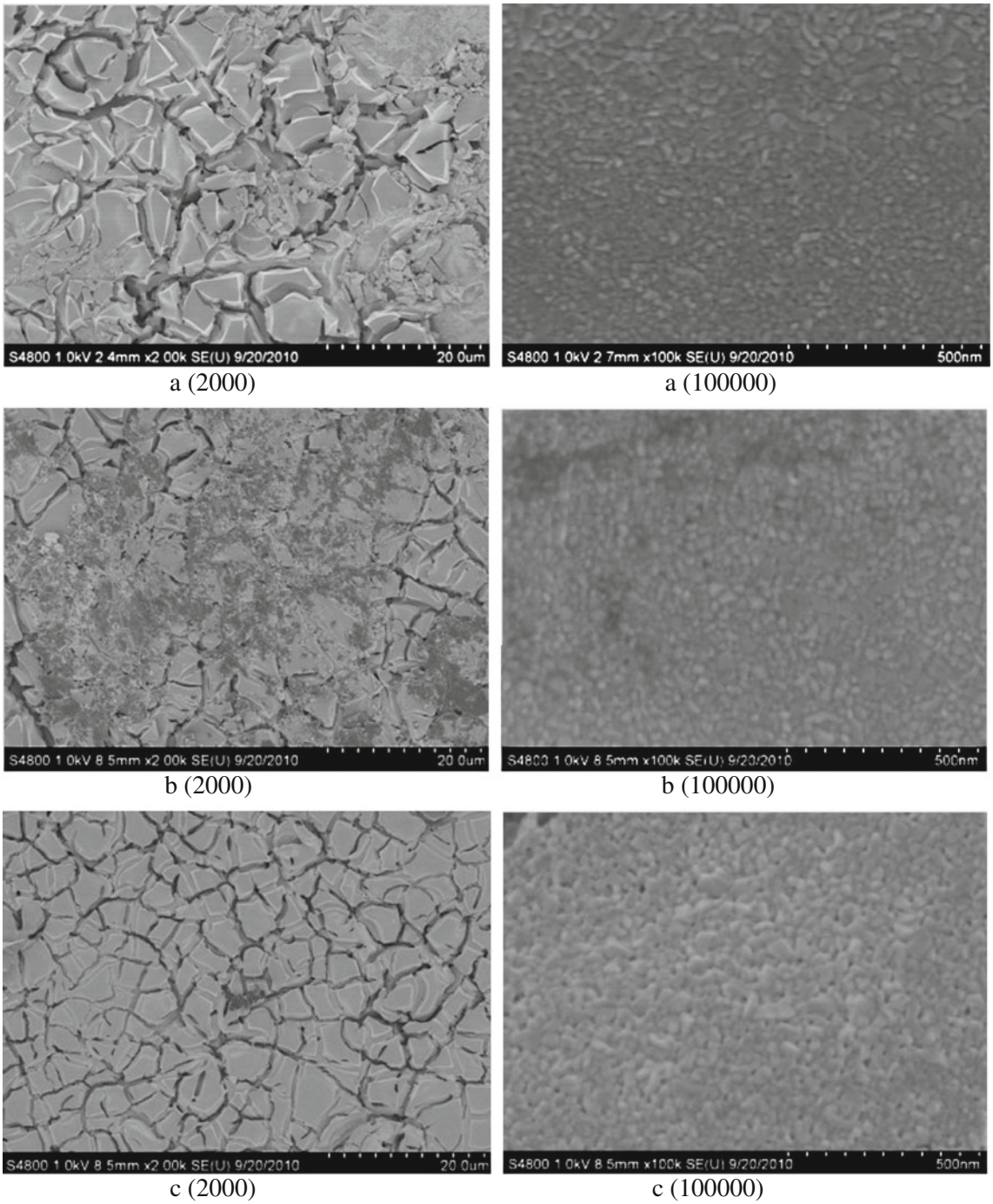

Fig. 18 SEM image of modified electrodes of TiO_2, Ce, and Ce–F

The modified powders were also tested under ultraviolet–visible diffuse reflection and the result was shown in Fig. 21 while the energy gap values were listed in Table 8. The absorption spectrum of co-doping electrode expanded to the visible light region but the extent was smaller than single Y-doping electrode, so the same to the data which resulted in energy gap, showing that F-doping cannot improve the photosensitivity of sunlight, which was in accordance with the published papers [35, 36].

EIS test was performed both under sunlight and UV light, and the results were shown in Fig. 22. Y–F co-doping and Y-doping revealed improvement under sunlight than no doping. The reason was that Y can improve the photosensitivity of visible light while F is taking advantage of separating h^+/e^- pairs; however, under UV light, the resistance of co-doping

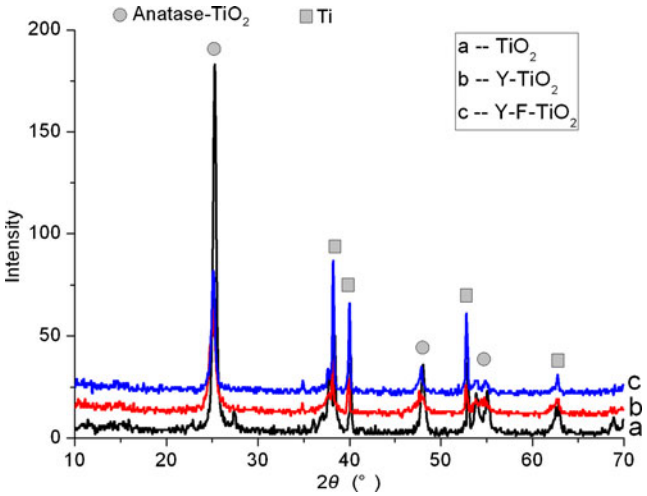

Fig. 19 XRD patterns of TiO_2, Y-doping TiO_2 and Y-F co-doping TiO_2 electrodes

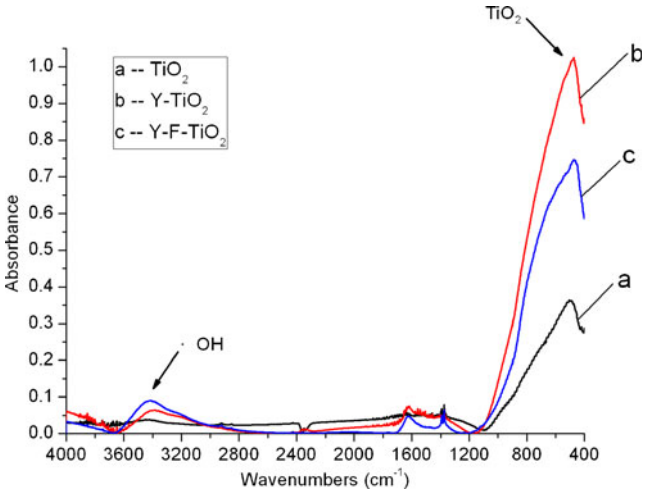

Fig. 20 FT-IR spectra of electrode under doping and co-doping of Y and Y-F

electrode was larger than under other conditions, which illustrated that co-doping was not conducive to UV light response but with enhanced sunlight response.

OCP was also tested here under UV light and the result was shown in Fig. 23. The figure exhibited that the OCP reached the biggest value at 0.7325 V under co-doping. Its response to UV lamp was also more notable than single doping and no doping, which proved that F can take effect on the separation of photo-generated h^+/e^- pairs so as to improve photosensitivity of electrode.

LSV was used for investigating the electrochemical properties as well. The conclusion can be seen as discussed in the following text (Fig. 24). Y–F co-doping and Y-doping showed their advantages under sunlight when the bias potential was smaller than 0.5 V because of the improvement of photosensitivity; under UV light, the photocurrent of co-doping was a little bit larger than that of other two electrodes, thanks to the separation effect of h^+/e^- pairs.

SEM was used for morphology and the pictures were displayed in Fig. 25. The results illustrated that under a magnification of × 2,000, the surface of single Y-doping electrode was much smoother and less cracked than that of Y–F co-doping or without doping, where the co-doping and no-doping electrode appeared with a typical cracking "island" structure; under the magnification of × 100,000, the grain size of single Y-doping electrode exhibited more refined particles with the value from 15 to 20 nm, where the Y–F co-doping made the lattice distortion more severe so as to make the grain size a little bit larger. However, the arrangement of particles was still dense and uniform and resulted in an increase of active sites and specific surface areas; on the contrary, the grain size of electrode without doping was not uniform and more cracks can be seen. Because no other oxides were found on the surface of electrodes, it proved that Y also joined in the lattice of the TiO_2 structure, replacing Ti^{4+}.

Given all that, the proper molar ratio of modified electrode with co-doping of Y and F should be nTi/nY= 100:1.0 and nTi/nF=1:0.1.

Table 7 Grain size of TiO_2, Y-doping TiO_2 and Y–F co-doping TiO_2 electrodes

Electrode	TiO_2	Y-doping TiO_2	Y–F co-doping TiO_2
Grain size, nm	19	15	19

Degradation on Disperse Blue solution under modified electrode

China was one of the largest dye-producing and dye-consuming countries in the world. Disperse dye was widely used among other kinds of dye. It had azo-bond (–N=N–) and

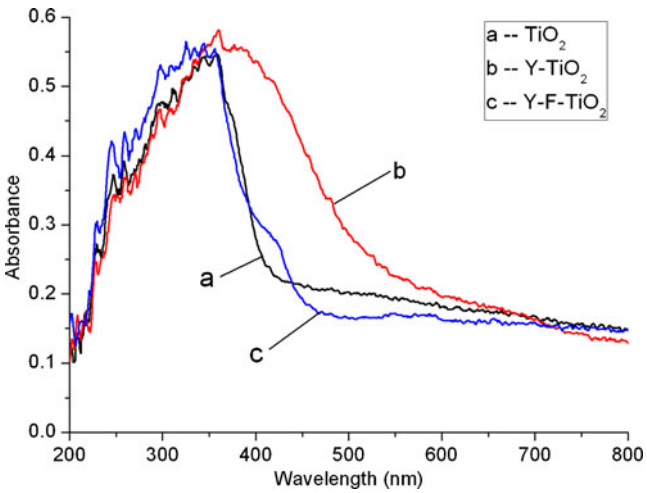

Fig. 21 UV–vis spectrum under different co-doping of Y and Y-F

Table 8 Energy gap under co-doping of Y and Y–F

Electrode	TiO_2	Y–TiO_2	Y–F–TiO_2
Energy gap, eV	2.78	2.09	2.65

could be decomposed into more than 20 kinds of carcinogenic aromatic amine to harm human and environment. The degradation of azo dye was the process of breaking down the azo-bond and production of intermediate products and then further degradation into final products [21].

In this paper, 50 mL 100 mg/L Disperse Blue 165–1 solution was chosen as the target pollutant because the ratio of biological oxygen demand to chemical oxygen demand was pretty slow, which means that it is difficult to be biodegraded. During degradation, the pH was not adjusted and the pH of the dye solution was 6.2. The concentration of supporting electrolyte NaCl is 0.1 mol/L, and the decolorization time lasted 30 min while the time interval of 5 min was set.

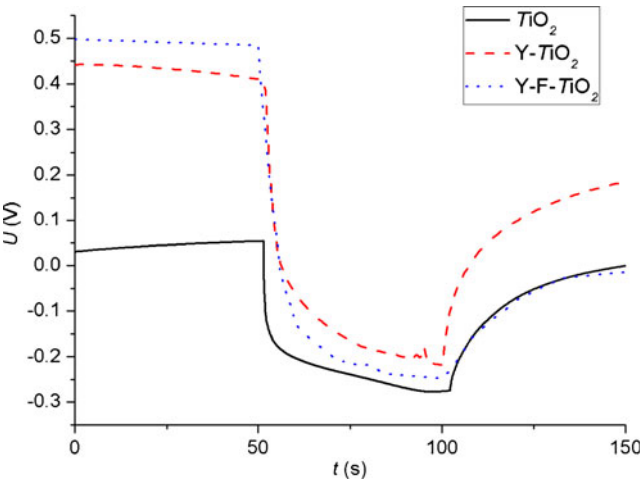

Fig. 23 Relationship between OCP and Y-doping or Y-F co-doping

Therefore, we discussed the optimal electrode for the final decolorization extent from different doping electrodes.

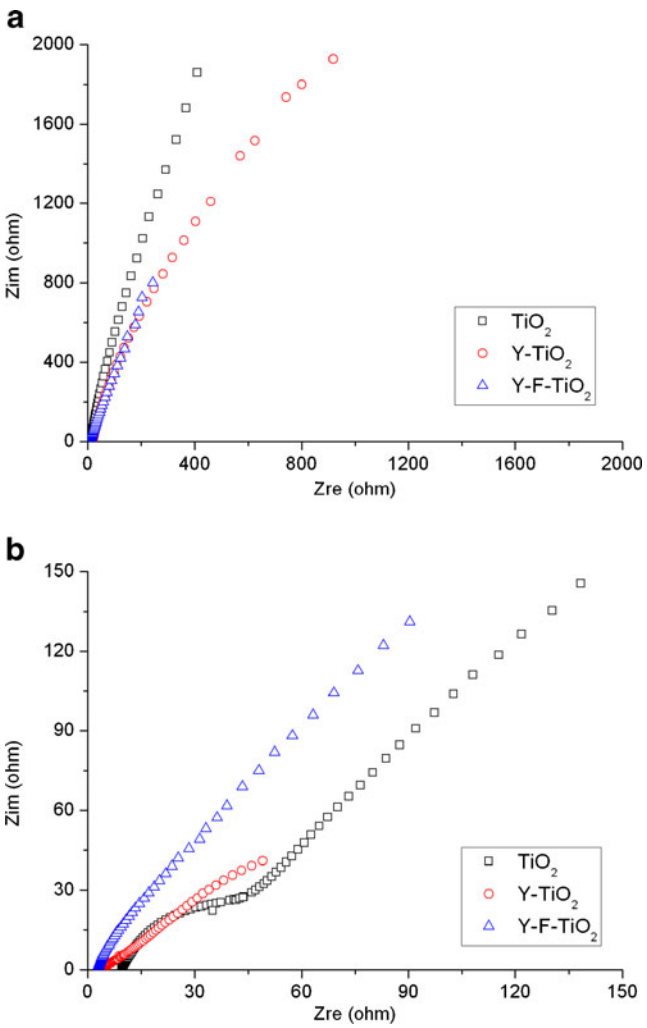

Fig. 22 EIS of electrode under co-doping of Y and Y-F

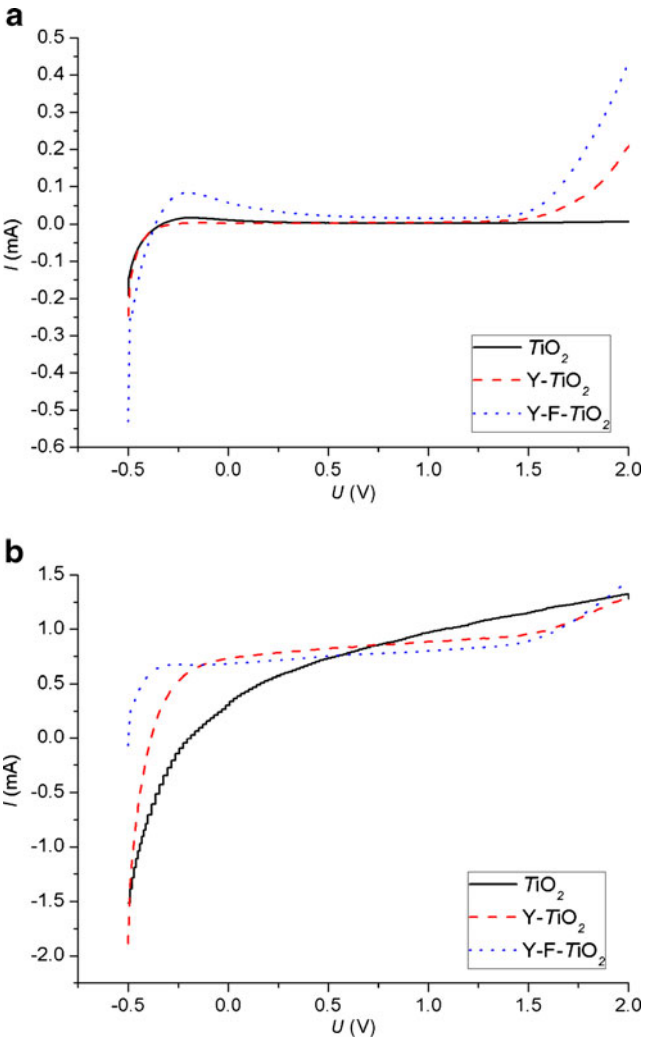

Fig. 24 LSV of electrode under co-doping of Y and Y-F

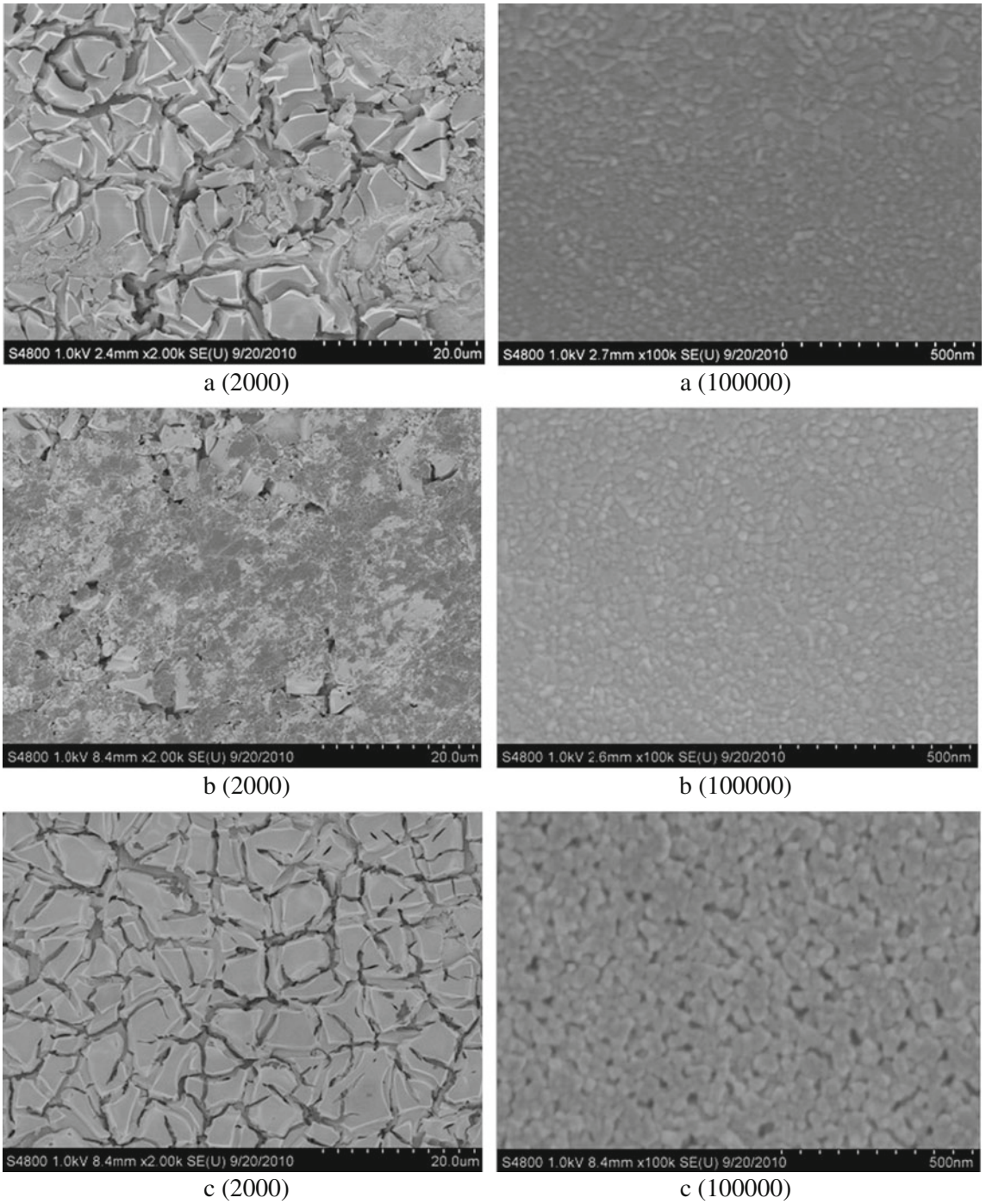

Fig. 25 SEM image of Y-doping and Y-F co-doping electrode

Influence of single doping on the photocatalytic degradation of DB

Degradation of DB by electrodes with single Y-doping and Ce-doping was researched under both sunlight and UV light. The result was shown in Fig. 26. Under sunlight, the lowest concentration after degradation was the Y-doping electrode with molar ratio at *n*Ti/*n*Y=100:1.0. The final residual concentration of DB was 88.38 mg/L, which meant that the decolorization extent was 11.62%. This resulted from the expanding of photosensitivity to the visible light region, the lower energy gap, the decreased electrode resistance as well as the larger response of OCP, whereas under UV light, the results were different from those under sunlight. Ce-doping with molar ratio at *n*Ti/*n*Ce=100:0.5 showed the optimal effect for degradation. The residual

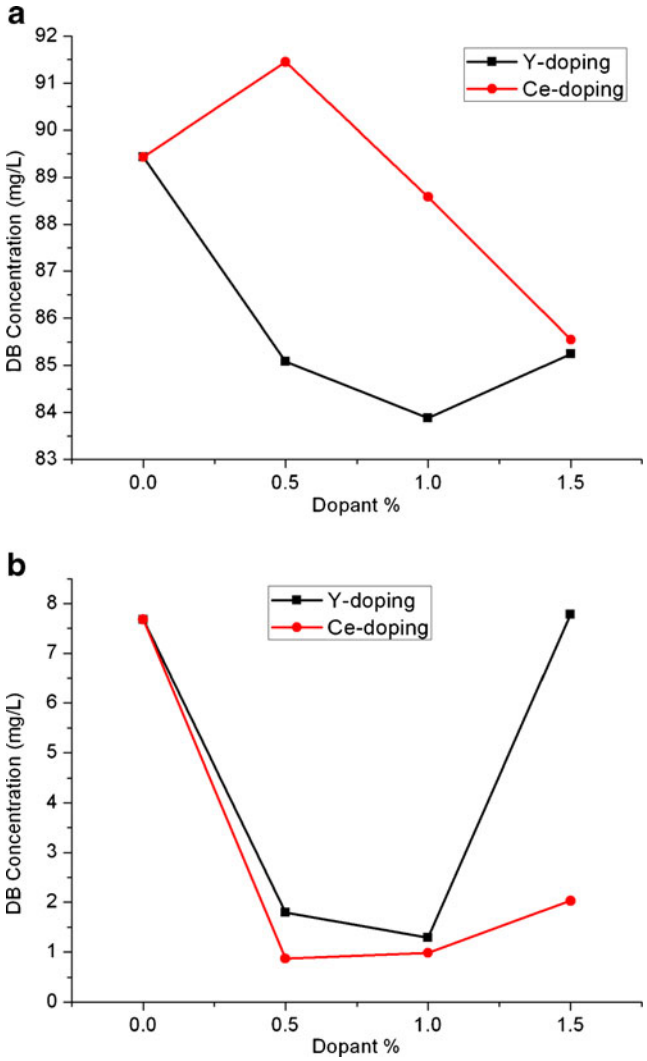

Fig. 26 Degradation of single doping electrodes on DB

concentration was only 0.87 mg/L after 30 min and the decolorization extent was more than 99%. This is attributed to the fact that Ce-doping refined grain size so as to increase the active sites and enhance the photocurrent. The conclusion was in accordance with the research from the property investigation as discussed earlier.

Influence of co-doping on the photocatalytic degradation of DB

Electrodes prepared under co-doping of Y, Ce, and F and single doping as well as no doping for degradation of DB both under sunlight and UV light were tested under the same conditions to avoid operation errors and environmental variations. The changes of relationship between DB concentration and time were drawn in Fig. 27.

The figures demonstrated that at the first 5 to 10 min, the concentration of DB decreased dramatically under different electrode degradation, which meant that the decolorization of DB was rapid during this time period. With time passing by, the DB concentration varied much smoother. Under sunlight, Y-doping and Y–F co-doping electrodes exhibited better effect than Ce-doping and Ce–F co-doping electrodes, respectively, and the effect of Y–F co-doping was even more notable than single doping. The final decolorization extent was 44.43% after 30 min. It was 30.77% higher than no doping, which embodied its improvement in expanding of photosensitivity due to the broadening of photosensitivity of Y^{3+} and the separation effect of F^{-}. The synergic effect showed obvious advantages than other electrodes, while under UV light, Ce–F co-doping electrodes showed the best performance in degradation of DB and the final decolorization extent was 96.86% after 30 min. This resulted from the lattice distortion and its contribution to lower the energy gap and resistance so as to produce a large amount of active sites to degrade organic dye solution.

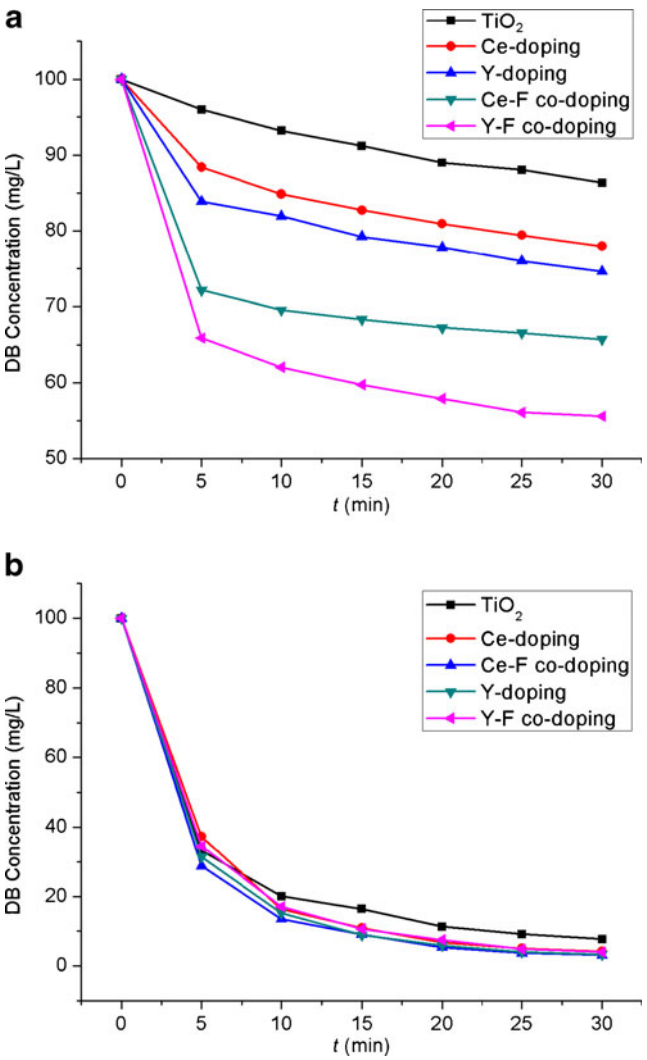

Fig. 27 Degradation of co-doping electrode on DB

Table 9 Kinetic parameters under different doping electrodes under sunlight

Doping electrode	k_1 L/mg	k_{obs} mg/(L min)	R^2
TiO_2TiO_2	0.0095	0.0577	0.9722
Ce-doping	0.0103	0.0675	0.9932
Ce–F co-doping	0.0116	0.0618	0.9554
Y-doping	0.0106	0.0694	0.9910
Y–F co-doping	0.0120	0.1578	0.9652

Table 10 Kinetic parameters under different doping electrodes under UV light

Doping electrode	k_1 L/mg	k_{obs} mg/(L min)	R^2
TiO_2	0.0138	5.2464	0.9973
Ce-doping	0.0119	6.0939	0.9531
Ce–F co-doping	0.0135	6.4674	0.9717
Y-doping	0.0127	6.0652	0.9701
Y–F co-doping	0.0119	6.0971	0.9779

Kinetic model for photocatalytic degradation of DB

Langmuir–Hinshelwood model was the general kinetic model for photo-catalytic degradation [21]. It could be expressed as follows:

$$r = -\mathrm{d}C/\mathrm{d}t = k_{obs} \times k_1 \times C/(1 + k_1 \times C) \quad (4)$$

where r is reaction rate [mg/(L min)], C is concentration of DB at any time (mg/L), t is reaction time (min), k_{obs} is apparent reaction rate constant [mg/(L min)], and k_1 is adsorption rate constant (L/mg).

Through integrating Eq. (3) with respect to time (t), we can obtain:

$$\ln(C_0/C)/(C_0 - C) = k_{obs} \times k_1 \times [t/(C_0 - C)] - k_1 \quad (5)$$

where C_0 is initial concentration of DB (mg/L).

Kinetic models under sunlight for degradation

Through the drafting between $\ln(C_0/C)/(C_0\text{-}C)$ and $t/(C_0\text{-}C)$, and Least Square Method was used to fit the kinetic parameters, the results of parameters were shown in Table 9, the data of k_{obs} showed that, it could reach the highest value under Y–F co-doping, which meant that the reaction rate was the fastest under this condition under sunlight. At the same time, the modification had influence on k_1, its value also reached the highest level under Y–F co-doping. As a result, Y–F co-doping was chosen as the best electrode for degradation under sunlight.

The comparison between theoretic fitting degradation curve derived from obtained k_{obs} and k_1 and experimental degradation data was also shown in Fig. 28, it turned out that the kinetic parameters fitted well with the real degradation.

Kinetic model under UV light for degradation

Also, through the drafting between $\ln(C_0/C)/(C_0{-}C)$ and $t/(C_0{-}C)$, least square method was used to fit the data shown in Table 10. The results of k_{obs} showed that it could reach the highest value under Ce–F co-doping, which meant that the reaction rate was the fastest under this condition. The modification had less influence on k_1. It did not vary notably among different electrodes. As a result, Ce–F co-doping was chosen as the best electrode for degradation under UV light.

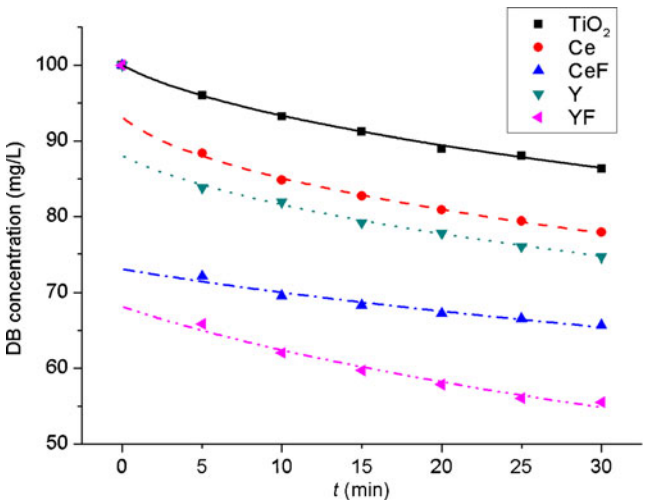

Fig. 28 Comparison between theoretical and real degradation under different electrodes under sunlight

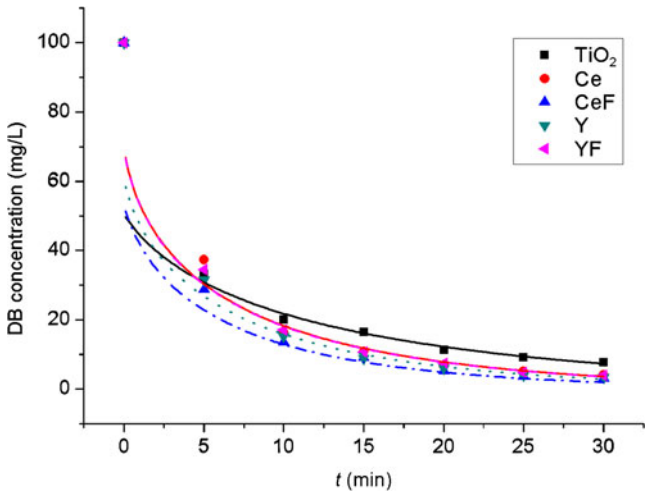

Fig. 29 Comparison between theoretical and real degradation under different electrodes under UV light

The comparison between theoretic fitting degradation curve derived from obtained k_{obs} and k_1 and experimental degradation data was also shown in Fig. 29. It turned out that the kinetic parameters fitted perfectly with the real degradation.

Conclusion

The following conclusions are hence drawn from this study:

1. Sol–gel method can be used for the preparation of modified nano-TiO_2 film electrode with nano-grain size and high photocatalytic activity. Cerium and yttrium can refine the grain size and take effect on expanding the photosensitivity to the visible light region while non-metal element fluorine serves for the effective separation of photo-generated h^+/e^- pairs so as to improve the final decolorization extent.
2. Under SEM, Autolab, XRD, FT-IR tests, and the like, the proper molar ratio for Ce–F co-doping is nTi/nCe=100:0.5 and nTi/nF=1:0.1 under UV light, while the proper molar ratio for Y–F co-doping is nTi/nY=100:1.0 and nTi/nF=1:0.1 under sunlight.
3. The modified co-doping electrodes were investigated for the degradation of 100 mg/L DB solution. The optimal final decolorization extent after 30 min under sunlight is 44.43% as tested by Y–F co-doping electrode and 96.86% under UV light as experimented by Ce–F co-doping electrode.
4. The kinetic model for degradation is well in accordance with the general Langmuir–Hinshelwood model. The bigger the k_{obs} and k_1, the faster the reaction and adsorption rate. In this paper, k_{obs} reaches the maximum value at Ce–F co-doping under UV light while under sunlight for Y–F co-doping. The theoretical degradation curve derived from kinetic parameters is also well matched with the real degradation.

Acknowledgements This work was supported by the Natural Science Foundation of Shanghai (No. 10ZR1432500) and Central Laboratory of Department of Chemistry and School of Life Science and Technology at Tongji University.

References

1. Shi YH, Meng HM, Sun Dongbai YuHY, Wang XD (2007) Progress of Ti based base metal oxide coating anode. J Funct Mater 38:2696–2699
2. P HQ, Xu K (2003) Current status and prospect of printing & dyeing waste-water treatment. Sichuan Textile Technology 2:11–14
3. Meng NC, Bo J, Christopher WK, Chris S (2010) Recent developments in photocatalytic water treatment technology: a review. Water Res 44:2997–3027
4. Fujishima A, Honda K (1972) Electrochemical photolysis of water at a semiconductor electrode. Nature 238:37–38
5. Yang HM, Zhang K, Shi RR, Li XW, Dong XD, Yu YM (2006) Sol–gel synthesis of TiO_2 nanoparticles and photocatalytic degradation of methyl orange in aqueous TiO_2 suspensions. J Alloys Compd 413:302–306
6. Uzunova M, Kostadinov M, Georgieva J, Dushkin C, Todorovsky D, Philippidis PI, Sotiropoulos S (2007) Photoelectrochemical characterisation and photocatalytic activity of composite La_2O_3–TiO_2 coatings on stainless steel. Appl Catal B-Environ 73:23–33
7. Marta M, William B, Colussi AJ, Michael R, Hoffmann (2004) Oxidative power of nitrogen-doped TiO_2 photocatalysts under visible illumination. J Phys Chem B 108:17269–17273
8. Michael R, Hoffmann STM, Choi WY, Detlef WB (1994) The role of metal ion dopants in quantum-sized TiO_2: correlation between photoreactivity and charge carrier recombination dynamics. J Phys Chem 98:13669–13679
9. Riassetto D, Holtzinger C, Messaoud M (2009) Mechanisms involved in the platinization of sol–gel-derived TiO_2 thin films. J Photoch Photobio A 202:214–220
10. Félix G, Ricardo G, Manuel A (2008) Photodegradation of the herbicide 2,4-dichlorophenoxyacetic. J Mol Catal A-Chem 281:119–125
11. Archanakar YRS, Caidyanathan S (2009) Improved photocatalytic degradation of textile dye using titanium dioxide nanotubes formed over titanium wires. Environ Sci Technol 43:3260–3265
12. Chen QF, Jiang D, Xu Y (2009) Visible region photocatalysis of Ce–Si/TiO_2 synthesized using sol–gel hydrothermal method. Acta Phys- Chim Sin 25:617–623
13. Romero DC, Torres GT, Arévalo JC (2010) Synthesis and characterization of TiO_2 doping with rare earths by sol–gel method: photocatalytic activity for phenol degradation. J Sol–Gel. Part Sci Technol 56:219–226
14. Jian ZC, Pu YY, Fang JZ (2010) Microemulsion synthesis of nanosized TiO_2 particles doping with rare-earth and their photocatalytic activity. Photochem Photobio 86:1016–1021
15. Arconada N, Durán A, Suárez S, Portela R, Coronado JM, Sánchez B, Castro Y (2008) Synthesis and photocatalytic properties of dense and porous TiO_2-anatase thin films prepared by sol–gel. Appl Catal B-Environ 86:1–7
16. Wang XW, Gang L, Chen ZG, Li F, Wang LZ, Lu GQ, Cheng HM (2009) Enhanced photocatalytic hydrogen evolution by prolonging the lifetime of carriers in ZnO/CdS heterostructures. Chem Commun 23:3452–3454
17. Jin W, Nyago TD, James L (2009) Origin of photocatalytic activity of nitrogen-doped TiO_2 nanobelts. J Am Chem Soc 131:12290–12297
18. Malato S, Fernandez-Ibanez P, Maldonado MI, Blanco J, Gernjak W (2009) Decontamination and disinfection of water by solar photocatalysis: recent overview and trends. Catal Today 147:1–59
19. Wu S, Yu T, Zhang Y (2009) Preparation of mixed rare earth doped Ti/TiO_2 electrode and its evaluation. Sci Technol Dev 40:106–107
20. Li MC, Shen JN (2006) Photoelectrochemical oxidation behavior of organic substances on TiO_2 thin-film electrodes. J Solid State Electr 10:980–986
21. Xiao SH, Qu JH, Liu HJ, Zhao X, Wan DJ (2009) Fabrication of TiO_2/Ti nanotube electrode and the photoelectrochemical behaviors in NaCl solutions. J Solid State Electr 13:1959–1964
22. Devi LG, Kottam N, Murthy BN (2010) Enhanced photocatalytic activity of transition metal ions Mn^{2+}, Ni^{2+} and Zn^{2+} doped polycrystalline titania for the degradation of Aniline Blue under UV/solar light. J Mol Catal A-Chem 328:44–52
23. Khan R, Kin SW, Kin TJ et al (2008) Comparative study of the photocatalytic performance of boron-iron co-doped and boron-doped TiO_2 nanoparticles. Mater Chem Phys 112:167–172
24. Zhang HR, Tan KQ, Zheng HW (2011) Preparation, characterization and photocatalytic activity of TiO_2 codoped with yttrium and nitrogen. Mater Chem Phys 125:156–160

25. Adel AI (2005) Synthesis and characterization of Y_2O_3–Fe_2O_3–TiO_2 nanoparticles by sol–gel method. Appl Catal B-Environ 58:115–121
26. Zhang XC, Yang HM, Tang AD (2008) Optical, electrochemical and hydrophilic properties of Y_2O_3 doped TiO_2 nanocomposite films. J Phys Chem B 112:16271–16279
27. Karunakaran C, Abiramasundari G, Gomathisankar P (2010) Cu-doped TiO_2 nanoparticles for photocatalytic disinfection of bacteria under visible light. J Colloid Interf Sci 352:68–74
28. Huang LF, Song N, Yao Y (2009) Progress in research of doping modification of nano-sized TiO_2 photocatalyst. Titanium Ind Process 26:22–25
29. Long R, English NJ (2009) Synergistic effects of Bi/S codoping on visible light-activated anatase TiO_2 photocatalysts from first principles. J Phys Chem C 113:8373–8377
30. Xu KJ, Zhu GQ (2009) Preparation and characterization of nano-La (S, C)-TiO_2 oriented films by template hydrothermal synthesis. Appl Surf Sci 255:6691–6695
31. Wang P, Liu ZR, Lin F (2010) Optimizing photoelectrochemical properties of TiO_2 by chemical codoping. Phys Rev A 82:1–4
32. Huang DG, Liao SJ, Liu JM (2006) Preparation of visible-light responsive N-F-codoped TiO_2 photocatalyst by a sol–gel-solvothermal method. J Photochem Photobio A-Chem 184:282–288
33. Montoya JF, Salvador P (2007) The influence of surface fluorination in the photocatalytic behaviour of TiO_2 aqueous dispersions-An analysis in the light of the direct–indirect kinetic model. Appl Catal B-Environ 94:97–107
34. Giannakopoulou T, Todorova N, Vaimakis T (2008) Study of fluorine-doped TiO_2 sol–gel thin coatings. J Sol Energy Eng 130:1–5
35. Yu CL, Zhou WQ, Yang K (2010) Hydrothermal synthesis of hemisphere-like F-doped anatase TiO_2 with visible light photocatalytic activity. J Mater Sci 45:5756–5761
36. Pelaez M, Cruz AA, Stathatos E (2009) Visible light-activated N-F-codoped TiO_2 nanoparticles for the photocatalytic degradation of microcystin-LR in water. Catal Today 144:19–25